A Dynamical Systems Model of the Dansgaard–Oeschger Oscillation and the Origin of the Bond Cycle

KOTARO SAKAI

Institute for Hydrospheric-Atmospheric Sciences, Nagoya University, Nagoya, Aichi, Japan

W. RICHARD PELTIER

Department of Physics, University of Toronto, Toronto, Ontario, Canada

(Manuscript received 24 November 1997, in final form 27 March 1998)

ABSTRACT

A low-dimensional dynamical systems model of the North Atlantic thermohaline circulation has been developed in order to better understand the mechanism underlying the so-called Dansgaard–Oeschger oscillation that is so clearly evident during the late glacial period (oxygen isotope stage 3) of the most recent ice-age cycle. The reduced system is designed to describe the evolution of the salinity distribution in this region that has previously been analyzed using both two- and three-dimensional models of the deep ocean circulation. The drastically simplified model described herein is shown to accurately represent the essence of the Dansgaard–Oeschger oscillation as this was previously revealed through detailed analyses performed with a model in which the deep circulation was described using a set of linked interacting two-dimensional (latitude–depth) basins. The authors' analyses with the reduced dynamical system reinforce their previous contention that the Dansgaard–Oeschger oscillation is driven by low–midlatitude salt accumulation and controlled by high-latitude freshening, as suggested in previous investigations performed with the more complex model. The dependence of the response of the reduced dynamical systems model to time-dependent external forcing is also investigated. These analyses demonstrate that the mechanism underlying the Dansgaard–Oeschger oscillation that is supported by the model is rather stable against relatively short timescale perturbations, but that the oscillation is effectively modulated by relatively long timescale perturbations such as those that Greenland ice-core data suggest to have existed on the timescale of successive Heinrich events. The dynamical systems model is thereby shown to provide a viable explanation of the Bond cycle that consists of packets of Dansgaard–Oeschger oscillations.

1. Introduction

Climate variability during the late Pleistocene epoch was unmistakably dominated by prominent 100 000-yr ice age cycles (e.g., Imbrie et al. 1984), each of which consisted of a relatively brief warm interglacial period followed by a considerably longer and increasingly cold glacial period that was terminated by a rapid warming that returned the system to the interglacial state. Recent investigations of the last glacial–interglacial cycle, however, have provided new information concerning the detailed characteristics of the glacial state. Isotopic analyses of Summit, Greenland, ice cores by the GRIP (1993) and GISP2 (1993) collaborations, in particular, demonstrate that the North Atlantic region experienced an intense millennial timescale climate oscillation during the late glacial period. This epoch, which extended from 60 kyr BP (1 kyr = 1000 years, BP = before present) to 35 kyr BP, is usually referred to as oxygen isotope stage (OIS) 3. When the time series of $\delta^{18}O$ variability in the Greenland ice cores is mapped into a history of atmospheric temperature change (e.g., Johnsen et al. 1992), one finds that the amplitude of the temperature change of the millennial timescale oscillation apparently exceeded 6°C, which is more than half of the glacial–interglacial temperature change itself in the North Atlantic geographical region. This millennial timescale oscillation, herein referred to as the Dansgaard–Oeschger (D–O) oscillation, is composed of a cycle that begins with a sudden warming from the cold glacial state toward warm quasi-interglacial conditions. The warm stage of a single cycle of the D–O oscillation may persist as long as several millennia after onsetting on a timescale as short as a century. Superimposed upon this basic D–O oscillation, there appears to be a further characteristic of the OIS 3 variability; Bond et al. (1993) have demonstrated that individual cycles of the D–O oscillation are apparently clustered so as to form a longer timescale sawtooth-shaped cycle with a timescale

Corresponding author address: Dr. W. Richard Peltier, Department of Physics, University of Toronto, 60 St. George Street, Toronto, ON M5S 1A7, Canada.
E-mail: peltier@atmosp.physics.utoronto.ca

© 1999 American Meteorological Society

Downloaded from http://journals.ametsoc.org/jcli/article-pdf/12/8/2238/3775210/1520-0442(1999)012_2238_adsmot_2_0_co_2.pdf by guest on 15 June 2020

of order 10^4 yr. This will be referred to herein as the Bond cycle. Each such Bond cycle has been shown to be initiated by an individual Heinrich event (Heinrich 1988). These events are defined in deep sea sedimentary cores from the North Atlantic as horizons containing large quantities of ice rafted debris. The Bond cycle thus consists of a modulation of the basic D–O oscillation in which the amplitude of successive D–O phases in a single Bond cycle gradually decreases. This $O(10^4)$ yr modulation of the D–O oscillation is very apparent in the ice core records, but the underlying mechanism has never been explained.

The evidence for the above-described D–O climate oscillation is not limited to that derived on the basis of proxies for temperature such as δ^{18}O in continental ice sheets. Keigwin and Jones (1994), for example, have demonstrated that similar variability existed in the North Atlantic (NA) Ocean that is well correlated with the Greenland oxygen isotopic information. Although the phase relation between the δ^{18}O time series measured by GRIP and GISP2, and the proxy for North Atlantic Deep Water (NADW) activity analyzed by Keigwin and Jones (1994) is still unclear, the role of the thermohaline circulation of the North Atlantic Ocean in the D–O oscillation would appear to be well established. Given the magnitude of the heat transferred to the atmosphere that accompanies the process of deep water formation, approximately 100 W m^{-2} on annual average (e.g., Bunker and Washington 1976; Hsiung 1986), it is clear that fluctuations in thermohaline circulation (THC) strength would be accompanied by large fluctuations in atmospheric temperature. The characteristic timescale of the deep ocean circulation is a further factor that suggests that the NADW formation process must be a very important contributor to long timescale climate variability, for the characteristic timescales that may be inferred from the geometry of the NA basin and the observed strength of the overturning circulation ($\sim$18 Sverdrups, 1 Sv $\equiv 10^6$ m^3 s^{-1}) range from centuries to millennia. This has been demonstrated explicitly in the recently published analyses of Sakai and Peltier (1997), hereafter referred to as SP97.

It is therefore very reasonable on physical grounds to hypothesize that the processes that are involved in NADW formation play a very important role in the D–O oscillation. If the oscillation were also observed under modern climate conditions, we could obtain much more detailed information that would enable us to clearly understand the underlying mechanisms. Following deglaciation, however, the large-amplitude millennial timescale climate variability corresponding to the D–O oscillation entirely disappeared, and only much weaker fluctuations have been observed through the current Holocene period (e.g., Stuiver 1980; GRIP 1993; GISP2 1993; but see Bond et al. 1997). Our detailed knowledge of the functioning of the late glacial climate regime during the last ice age cycle thus remains rather limited. In this circumstance, perhaps the only means we have at our disposal by which to better understand late glacial climate is through the construction of appropriate mathematical models of the climate system that are integrated subject to appropriate boundary conditions.

The timescale of a typical cycle of the D–O oscillation, which ranges from a millennium to several millennia, is still sufficiently long as to make the use of full three-dimensional atmosphere–ocean general circulation models prohibitive due to present limitations on the availability of computational resources. Only very limited analyses of this kind have been performed; the work of Winton and Sarachik (1993) provides one example based upon the use of a modestly configured ocean general circulation model that demonstrated that the intense millennial timescale oscillations of the thermohaline circulation were possible under appropriate conditions but no possible link to the D–O oscillations was recognized or considered. Concerning the previously discovered THC oscillation that consists of ''flush'' and ''collapse'' phases, which was originally discovered by Marotzke (1989) and later rediscovered in a three-dimensional ocean general circulation model by Weaver et al. (1993), this work was primarily focused on century timescale variability and again no possible connection of the flush–collapse oscillation to the Dansgaard–Oeschger oscillation was recognized. Because of the computational resources that would be required to perform the tens of thousands of year integrations needed to fully investigate this phenomenon, there is clearly an important role to be played by dimensionally reduced models of the physical process. Such models are capable of being integrated over such long timescales and may therefore serve an extremely useful purpose.

Sakai and Peltier (1995, 1996), the latter of which will hereafter be referred to as SP96, have in fact recently developed a model of this type and have performed a variety of analyses with it. Their model of the global THC consists of a linked set of two-dimensional basins in which a thermohaline circulation develops in response to surface forcing that may be taken to represent either glacial or interglacial (modern) conditions. In the context of the analyses of the D–O oscillation performed with this model, it has been successfully demonstrated that the THC is actually expected to oscillate on precisely the D–O timescale even under steady boundary conditions characteristic of the late glacial state. The more recent work described in SP97 further embellished this original analysis. Whereas the former investigations were performed with an ocean-only version of the model, in SP97 the multibasin model of the THC was coupled to a global model of the atmosphere and further detailed reanalyses of the D–O oscillation performed. The results obtained with the coupled model clearly show that the intense oscillation of THC drives an oscillation of atmospheric temperature of precisely the amplitude inferred on the basis of oxygen isotope data from the Greenland ice cores. Furthermore, the form of the oscillation delivered by the coupled model

Downloaded from http://journals.ametsoc.org/jcli/article-pdf/12/8/2238/3775210/1520-0442(1999)012_2238_adsmot_2_0_co_2.pdf by guest on 15 June 2020

was found to be in much closer accord with the ice core–based inference than that obtained with the ocean-only version of the model.

According to the results obtained in these analyses, a cycle of the millennial timescale oscillation of the THC, which comprises the oceanic component of the D–O oscillation, consists of two entirely distinct stages: one involving intense NADW formation, and a second in which very little NADW is produced at all. During a typical intense stage of NADW formation, the warm saline water that constitutes the upper layer of the low–midlatitude North Atlantic is transported northward, cooled, and sinks to form NADW. When the surface freshening of the high-latitude NA is increased, due, say, to enhanced surface runoff from the ice sheets, a more intense overturning circulation is required to provide sufficient salt to sustain the strength of the THC. In the presence of such THC overintensity, midlatitude high-salinity water becomes strongly depleted of salt, which causes the circulation to be arrested; in this state deep water becomes stagnant. In the stagnant state of the deep circulation, little high-salinity water is removed from midlatitudes, and salt accumulation builds up, leading eventually to an unstable state in which deep water abruptly begins to form once more. The model therefore provides a detailed fluid mechanical proof of the *salt oscillator* concept that had previously been hypothesized on qualitative grounds and establishes that the conditions required for its operation are precisely those that are expected to have obtained under full glacial conditions.

If the quantitative picture at the Dansgaard–Oeschger oscillation provided by this previous work is correct, it is sufficiently simple that we should be able to describe the essence of the physical process using a mathematical structure that is further reduced from that of the multi-two-dimensional basin ocean model employed in these original analyses. The purpose of this paper is to develop this further reduced form of our theory of the D–O oscillation and to employ the reduced theory to provide an initial investigation of the Bond cycle.

In section 2, we formulate the *dynamical systems* model of the NA THC that will be investigated thereafter. In section 3 we discuss the equilibrium solutions of the reduced system and analyze their linear stability. The analyses presented in this section also demonstrate the existence of a regime of nonsteady solutions in the control parameter space of the model, which is of course required if the model is to support an oscillatory solution of the kind required to understand the D–O oscillation. In section 4 we show typical integrations of the model in the region of parameter space in which it delivers oscillatory solutions on the millennial timescale. Section 5 briefly describes the response of the dynamical systems model of the North Atlantic THC to a range of periodic perturbations, the period of which ranges from $O(1)$ to $O(10^5)$ yr. Our conclusions are summarized in section 6.

2. A new dynamical systems model of the North Atlantic thermohaline circulation

The deep ocean thermohaline circulation is a hydrodynamic flow driven by density variations in which the (potential) density of sea water is primarily controlled by two variables, namely, the temperature and salinity. Although the potential temperature is almost a materially conserved quantity in the deep ocean, that of the upper mixed layer is strongly influenced by the surface distribution of atmospheric temperature. The salinity distribution, on the other hand, is not so strongly controlled by atmospheric conditions, mainly due to the absence of feedbacks involved in the processes of evaporation, precipitation, and runoff from the continents that control sea surface salinity. Although it is the density distribution that controls the THC flow, we primarily attribute it to variations of salinity for this reason. The influence of temperature variations will be included implicitly in the following discussion through two means: the first of these will be via the assumption that it is in the high-latitude cold region of the North Atlantic where NADW forms, whereas the second is that weak damping (based upon the use of a characteristic time that is short compared with that employed in control case analyses) due to air–sea interaction may be employed in place of the strong damping that we use in the standard analyses. One may, for the most part in this paper, therefore interchange the word *density* for the word *salinity* wherever it appears except in the scaling analyses.

a. Formulation of the model

In formulating the dynamical systems model that we will employ to capture the essence of the Dansgaard–Oeschger oscillation, it is useful to start from the general form of the advection–diffusion equation for salinity as

$$\frac{\partial s}{\partial t} + \mathbf{v} \cdot \nabla s = S + \mathcal{D}s. \tag{1}$$

This equation may be expressed in spectral form by introducing a complete set of basis functions as

$$\frac{\partial s_i}{\partial t} = S_i + \sum_j D_{ij} s_j - \sum_{j,k} A_{ijk} s_j \Psi_k. \tag{2}$$

Here we choose to take a somewhat empirical and a posteriori ''box-model'' approach to obtaining the appropriate basis functions. Based upon the analysis in SP97, the question of which subdomains of the ocean play actively important roles in the D–O oscillation is already understood: it is the upper layer water of the low–midlatitude North Atlantic as well as the high-latitude region in which NADW forms to drive the THC and the abyssal water itself that have been established as being principally involved. We will therefore choose box-model basis functions that are nonzero over these domains but otherwise vanish. Furthermore, we will re-

Downloaded from http://journals.ametsoc.org/jcli/article-pdf/12/8/2238/3775210/1520-0442(1999)012_2238_adsmot_2_0_co_2.pdf by guest on 15 June 2020

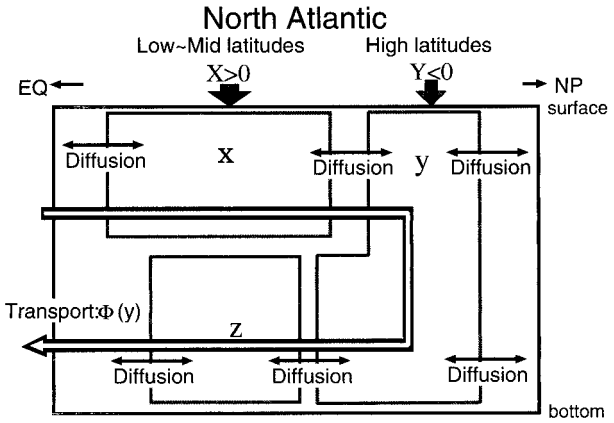

FIG. 1. Schematic overview of subdomain dividing in the NA for the reduced dynamical system model of the NA THC. The boxes indicate the extent of nonzero distribution for each component.

strict consideration to only these subdomains in developing this reduced description of the THC.

Figure 1 schematically illustrates the way in which the North Atlantic basin is subdivided based upon those considerations. We employ three corresponding basis functions to represent this division, which are such that on each subdomain the basis is assumed to be positive but otherwise is zero. Region 1 denotes the upper domain, which includes the low–midlatitudes of the North Atlantic, whereas region 2 represents the high-latitude domain in which the North Atlantic THC is driven by the production of NADW, and region 3 represents the abyssal water, which is included in order to allow us to represent the spatial heterogeneity in NADW.

The diffusive exchange between those subdomains of the basin will be assumed to be controlled by Fick's law and idealized in terms of two parameters, K and L, in which K is the coefficient controlling diffusive exchange between each of the domains (1, 2, 3) and the background water and L is the coefficient controlling exchange between the subdomains (1, 2, 3) themselves. One may then immediately assert the following governing equations for salinity of our somewhat idealized model of the North Atlantic THC based upon (2) as

$$\frac{ds_1}{dt} = R_1 - K(s_1 - s_{bg}) - L(s_1 - s_2) - \Phi(s_2)(s_1 - s_{bg}) \quad (3)$$

$$\frac{ds_2}{dt} = R_2 - 2K(s_2 - s_{bg}) - L(s_2 - s_1) - L(s_2 - s_3) - \Phi(s_2)(s_3 - s_1) \quad (4)$$

$$\frac{ds_3}{dt} = -K(s_3 - s_{bg}) - L(s_3 - s_2) - \Phi(s_2)(s_3 - s_2), \quad (5)$$

in which we will hereafter assume that the transport function Φ assumes the following simple form:

$$\Phi = \begin{cases} \alpha|s_2 - s_{bg}|^\beta & \text{if } s_2 > s_{bg} \\ 0 & \text{otherwise.} \end{cases} \quad (6)$$

In the event that $\beta = 1$, the THC is then linearly proportional to salinity differences, as is approximately the case in existing two-dimensional THC models such as that of SP96. This is expected to be a highly simplified representation of actual THC transport. The factor 2 that appears in the first diffusion term in the governing equation for the salinity of region 2 is rather artificially introduced to simplify the analytical procedure. We have performed several sets of numerical integrations with different values of this factor (not shown in this paper) and thereby obtained essentially the same conclusions as will be discussed in what follows.

It is useful to nondimensionalize this system in order to clarify its mathematical structure. Such nondimensionalization may be performed using the following representations, which define new independent variables x, y, and z: $s_1 - s_{bg} = s_0 x$, $s_2 - s_{bg} = s_0 y$, $s_3 - s_{bg} = s_0 z$, $t = \tau t^*$, $\tau = (K + L)^{-1}$, $\mu = L/(K + L)$, and $s_0^\beta = (K + L)/\alpha$. This nondimensionalization reduces the governing ordinary differential equations to the much simplified forms

$$\frac{dx}{dt^*} = X - x + \mu y - |y|^\beta x \quad (7)$$

$$\frac{dy}{dt^*} = Y - 2y + \mu(x + z) + |y|^\beta(x - z) \quad (8)$$

$$\frac{dz}{dt^*} = -z + \mu y + |y|^\beta(y - z). \quad (9)$$

Here the $|y|^\beta$ terms will be assumed to vanish when y is negative. The timescale τ may be roughly evaluated as follows: based upon the assumption that it is controlled by lateral diffusion, the basinwide salinity distribution changes over a length scale of $O(10^6)$~$O(10^7)$ m and a typical eddy-diffusion coefficient employed in low-resolution ocean general circulation models in which mesoscale eddies are not resolved is $O(10^2)$~$O(10^3)$ m^2 s^{-1} (e.g., Bryan and Lewis 1979). This leads to the previously stated characteristic timescales ranging from decades to millennia, when the square of the characteristic length is divided by the characteristic value of the diffusion coefficient. Similarly, based upon the intensity of vertical diffusion, and by using a typical depth of the thermocline layer of the ocean, for example, $O(10^3)$ m (e.g., Levitus 1982), and a typical vertical diffusion coefficient for this layer, for example, $O(10^{-4})$ m^2 s^{-1} (e.g., Bryan and Lewis 1979), one may obtain a second estimate of the characteristic timescale that turns out to be several hundred years.

b. The physically plausible region of parameter space

The value of μ is expected to lie in the range from zero to unity based upon the above definition and the

Downloaded from http://journals.ametsoc.org/jcli/article-pdf/12/8/2238/3775210/1520-0442(1999)012_2238_adsmot_2_0_co_2.pdf by guest on 15 June 2020

positive definiteness of the diffusive exchange coefficients. If the diffusive exchange between the domains (1, 2, 3), and that between the domains (1, 2, 3) and the background water are not of radically different intensity, then μ should be close to the value 0.5.

The forcing terms that we have added to the above system, that is, X and Y, which respectively derive from R_1 and R_2 in (3)–(5), are at least constrained with respect to sign on the basis of the observed distribution of evaporation minus precipitation over the surface of the North Atlantic Ocean (e.g., Peixoto and Oort 1992). Here X represents the salinity forcing over low–midlatitudes where very strong evaporation is caused by the subtropical atmospheric divergence, and it should therefore have a relatively large positive value. In dimensional form R_1 is of the order of 1 m yr^{-1} when it is expressed in terms of evaporation minus precipitation. Parameter Y corresponds to the salinity forcing over the high-latitude North Atlantic, where the combined influence of precipitation and surface runoff from the surrounding continents produce a negative salinity forcing so that Y should have a negative value when boundary conditions are realistic. In their nondimensional forms, X and Y are expected to lie in a certain range constrained by modern observations. The overall salinity of the oceans is not far removed from 0.035 g kg^{-1}. The global THC, however, is driven by very small differences of density (and thus salinity). We may quite safely assert that the deep water formation process that drives the THC is induced by relative differences in salinity of 10^{-1} or 10^{-2}. This leads directly to an estimate of the amplitude of the nondimensional forcing functions X and Y, namely, they should be close to the inverse of the relative differences, that is, of the order of 10^1 to 10^2. Later we will see that it is not the absolute amplitudes of X and Y but rather the ratio Y/X that determines the nature of the solutions to this dynamical systems representation of the North Atlantic THC.

In terms of the power low exponent β that appears in the representation of THC transport, it is expected not to be greatly different from unity considering that successful existing 2D THC models exist that are based upon the assumption of a proportionality between pressure gradient and velocity. Clearly there should be no THC-induced transport at all if there is no density gradient. It must therefore follow that the THC transport in the governing system can vanish when y is negative.

Before closing this section, we briefly review the relationship between the dynamical systems model of the THC just described and low-dimensional models of the THC that have been developed by others. The first example of interest is that by Stommel (1961) in terms of which the existence of multiple equilibria in the THC was first demonstrated. For the problem of the large-scale thermohaline circulation, the influence of double diffusion may be ignored and Stommel's model in nondimensional form may be written as

$$\frac{d\sigma}{dt} = 1 - \sigma - a|\sigma|\sigma,$$

in which σ is the density difference nondimensionalized by the forcing of the two boxes. Our model can be reduced to Stommel's model when x is held fixed to the value of background water, $z = y$, and $\mu = 1$ (renondimensionalization required); Stommel's model may then be seen to represent an idealized circumstance in which midlatitude salinity is assumed constant and NADW is homogeneous. Investigations using multibox models of the THC that are somewhat similar to our own, however, continue to provide interesting insight into a variety of ocean dynamical problems. One of the most recent contributions in this kind is that by Gargett and Ferron (1996). This work was focused upon the problem of double diffusion rather than upon the long timescale evolution of the large-scale THC. Employing a four-box THC model, they demonstrated the plausible existence of an instability that supports periodic solutions of century timescale and that is closely related to equatorial convective events. Another example of the application of models in this class is that by Nakamura et al. (1994) in which the influence of atmospheric feedback was incorporated into a three-box model of the THC and employed to demonstrate that the system may be destabilized by atmospheric eddy transports of both heat and moisture such that a steady state of intense NADW formation might be transformed to an essentially stagnant state. The possible existence of such a connection between the atmosphere and the THC may require us to modify our analysis of the bifurcation point beyond which a THC oscillation begins (as presented in SP96 and SP97) and will warrant attention in our future work.

There have also been a number of interesting contributions to the understanding of the THC using ''hula hoop'' models. Since models with this geometry are relatively easily analyzed, both analytically and quasi-analytically, and may also yield insights, they have often been invoked. Winton and Sarachik (1993) suggest that the oscillation that is observed as a limit cycle in the loop model may be the mechanism underlying the century timescale weak oscillation in their three- and two-dimensional fluid dynamical models. A most recent analysis of this kind is that by Huang and Dewar (1996), in which they have presented chaotic solutions of the loop model of the THC as well as periodic solutions (limit cycles). The loop model has therefore been employed primarily in the context of analyses of the variability of the THC on century or shorter timescales.

Aside from the above-mentioned box models of the THC, a number of climate models have been proposed that support oscillations on timescales longer than centuries. One example that is especially strongly connected to the Dansgaard–Oeschger oscillation is a model that combines an ice sheet component with an Atlantic THC component and that was discussed by Broecker et

Downloaded from http://journals.ametsoc.org/jcli/article-pdf/12/8/2238/3775210/1520-0442(1999)012_2238_adsmot_2_0_co_2.pdf by guest on 15 June 2020

al. (1990) and by Birchfield and Broecker (1990). The oscillation in this model is enabled by incorporating meltwater produced by runoff from the continental ice sheets onto the surface of the Atlantic ocean. The THC in this model is actually independent of the salinity distribution within the Atlantic basin and thus is free of even the lowest-order THC dynamics. Considering that our box-model analyses are being designed to reproduce the results obtained with the more complex hydrodynamic models, the ice sheet–salinity oscillator model developed by these authors is clearly fundamentally different from our own. Their analyses were nevertheless directed toward the development of a salt oscillator of the same kind as we have discovered to exist in the ocean-only version of our own model, where the THC is forced by an appropriate high-latitude freshwater anomaly that is presumably due to ice sheet runoff. The oscillation mechanism in our model of the THC does not require any coupling to the freshwater runoff from the continental ice sheets that controls the onset and shutdown of NADW formation in the model of Birchfield and Broecker.

3. Equilibrium solutions and their linear stability

In the present section our purpose will be to explore the properties of the equilibrium solutions of the box model of the THC embodied in (7)–(9). These will be enumerated and their stability properties explored.

Equilibrium solutions

Because of its simplicity, the dynamical systems model embodied in (7)–(9) is amenable to analytical characterization. The equilibrium solutions of this reduced model are those that obtain when the left-hand sides of the equations (7)–(9) are set to zero, namely,

$$0 = X - x + \mu y - |y|^{\beta} x \tag{10}$$

$$0 = Y - 2y + \mu(x + z) + |y|^{\beta}(x - z) \tag{11}$$

$$0 = -z + \mu y + |y|^{\beta}(y - z). \tag{12}$$

Recall that the $|y|^{\beta}$ terms are assumed to vanish when y is negative. Considering first the case in which $y < 0$, the system reduces to a linear system in x, y, and z. The solution, (x_{0l}, y_{0l}, z_{0l}), may be written as

$$x_{0l} = \frac{2 + \mu Y - \mu^2 X}{2(1 - \mu^2)} \tag{13}$$

$$y_{0l} = \frac{Y + \mu X}{2(1 - \mu^2)} \tag{14}$$

$$z_{0l} = \frac{\mu(Y + \mu X)}{2(1 - \mu^2)}. \tag{15}$$

Since $y_{0l} < 0$, the conditions $0 < \mu < 1$ and $Y + \mu X < 0$ are required in order that the solution remain physical. The meaning of the latter condition is that, when it obtains, the high-latitude NA is receiving too much freshwater to allow for the maintenance of an intense NA THC. The local stability of this equilibrium solution is determined by the characteristic equation

$$(\lambda + 1)(\lambda^2 + 3\lambda + 2 - 2\mu^2) = 0, \tag{16}$$

in which λ denotes the rate of exponential growth of a small-amplitude fluctuation superimposed upon the equilibrium solution. Apparently the equilibrium solution (x_{0l}, y_{0l}, z_{0l}) is always locally stable and thus represents the global attractor regardless of the sign of $Y + \mu X$.

When $y \geq 0$, (10), (11), and (12) yield the following solution for the nonlinear equilibrium (x_{0n}, y_{0n}, z_{0n}):

$$x_{0n} = \frac{X + \mu y}{1 + y^{\beta}}, \tag{17}$$

$$z_{0n} = \frac{\mu y + y^{\beta+1}}{1 + y^{\beta}}, \tag{18}$$

and

$$y_{0n}^{2\beta+1} + (2 - \mu)y_{0n}^{\beta+1} - (Y + X)y_{0n}^{\beta} + 2(1 - \mu^2)y_{0n} - (Y + \mu X) = 0. \tag{19}$$

When $\beta = 1$, (19) may be solved analytically and delivers three solutions. Any solution for y_{0n} that is either negative or complex is aphysical. We will therefore be interested only in the real positive solutions and their linear stability.

Suppose that we have found such an equilibrium solution (x_{0n}, y_{0n}, z_{0n}), then the corresponding linearized system, which determines the fate of small-amplitude fluctuations superimposed upon it, is

$$\frac{dx'}{dt^*} = -(1 + y_{0n})x' + (\mu - x_{0n})y' \tag{20}$$

$$\frac{dy'}{dt^*} = (\mu + y_{0n})x' + (x_{0n} - z_{0n} - 2)y' + (\mu - y_{0n})z' \tag{21}$$

$$\frac{dz'}{dt^*} = (\mu + 2y_{0n})y' - (1 + y_{0n})z', \tag{22}$$

so that the exponential growth rate λ of a small-amplitude perturbation is determined by the characteristic equation

$$(\lambda + 1 + y_{0n})(\lambda^2 + \alpha_1\lambda + \alpha_2) = 0 \tag{23}$$

with

$$\alpha_1 = 3 + y_{0n} + z_{0n} - x_{0n} \tag{24}$$

$$\alpha_2 = (1 + y_{0n})(1 + z_{0n} - x_{0n}) - (\mu - x_{0n})(\mu - y_{0n}) - (\mu - y_{0n})(\mu + 2y_{0n}). \tag{25}$$

Obviously one of the eigenvalues is negative when $y_{0n} > 0$. The remaining two eigenvalues are also negative

Downloaded from http://journals.ametsoc.org/jcli/article-pdf/12/8/2238/3775210/1520-0442(1999)012_2238_adsmot_2_0_co_2.pdf by guest on 15 June 2020

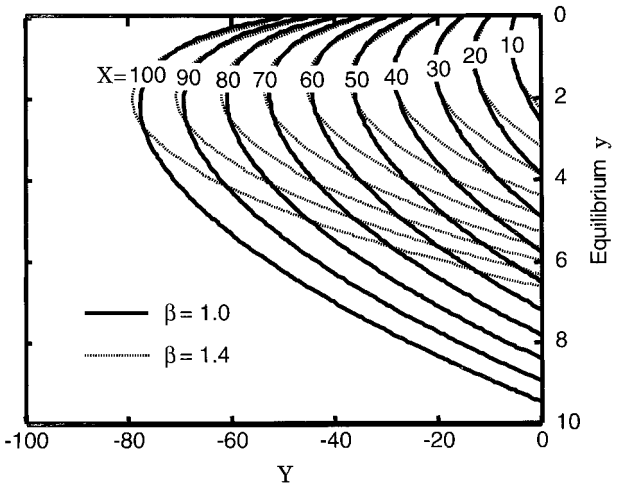

FIG. 2. Equilibrium solutions for y under different X and Y. Two cases for different values of β (1.0 and 1.4) are shown.

if $\alpha_1 < 0$ and $\alpha_1^2 < 4\alpha_2$, or if $-\alpha_1 + (\alpha_1^2 - 4\alpha_2)^{1/2} < 0$. When the real part of any of the eigenvalues is positive, the equilibrium is locally unstable. Although the existence of a locally stable solution does not guarantee that the solution will be a global point attractor, the nonexistence of a locally stable solution generally means there exist either orbits or chaotic attractors in the system so long as the solution can be shown to be bounded.

Before we proceed with further analysis, it will therefore be useful to determine whether or not solutions of the system remain bounded. Returning to the original system, (7)–(9), in the domain in which $y < 0$, the transport terms vanish. In this domain, z is bounded if y is bounded, and so in what follows we will assume that z remains near y. Any solution converges to the equilibrium solution if there exists a stable equilibrium solution in the $y < 0$ domain, and thus the solution is bounded in this case. Even if an equilibrium solution does not exist in the $y < 0$ domain, solutions in the $y < 0$ domain do not diverge. From (16), y_{0l} appears to attract all the solutions in the $y < 0$ domain even when $y_{0l} \geq 0$, in which case all solutions in the $y < 0$ domain shift to the complementary domain ($y \geq 0$).

When $y \geq 0$, on the other hand, the transport terms become important. From the evolution equation for x, $dx/dt^* < 0$ for all x if X, μ, $y > 0$: all the solutions initially in $y \geq 0$, $x < 0$ eventually enter the first quadrant. The only remaining question, then, is whether or not all the solutions in the first quadrant are bounded. Indeed, they are bounded if $\beta \geq 1$: first, the solution is bounded in the $x > 0$ direction. From (7), for all $y > 0$, there exists an $x_b > 0$ such that $dx/dt^* < 0$ for all $x > x_b$. Eventually, all solutions remain in the domain to the *left* of the curve,

$$x = \frac{X + \mu y}{1 + y^{\beta}}. \tag{26}$$

For $y \gg 1$, this behaves asymptotically as $x \sim \mu y^{1-\beta}$. Second, solutions remain bounded in the $y > 0$ direction. From (9), for a given x there exists y_b such that the equation eventually yields large $z_b \sim y_b$, $z_b \gg x$ after a certain time [x eventually remains in the domain to the left of the curve (26)]. Since x cannot be very large for large y_b, the diffusion term remains negative, while the transport term assumes a large negative value. This is true for all $y > y_b$.

This analysis demonstrates that the dynamical systems model consisting of (7), (8), and (9) has a stable equilibrium solution when $Y + \mu X < 0$ in the $y < 0$ domain, and that, regardless of the local stability of the equilibrium solutions in $y \geq 0$, all the solutions are bounded so that the solution is expected to become an orbit (possibly a limit cycle) or to become chaotic when the equilibrium solution is locally unstable. In the remainder of this section we will present a detailed discussion of the previously discussed linear analyses. If all of the equilibrium solutions were stable, then the situation is expected to be very similar to that originally discussed by Stommel (1961), who for the first time demonstrated the existence of multiple equilibria in a simple dynamical systems model of the thermohaline circulation. In Stommel's analysis the system that he constructed allowed only point attractors that correspond to steady states. We will herein demonstrate that both steady multiple equilibrium solutions and nonsteady bounded solutions can exist in the present model depending upon the choice of parameters.

In this investigation, we will be primarily concerned with the dependence of the behavior of the dynamical system upon the two forcing parameters, namely, X and Y, and the impact of these parameters will be examined over the range $X \in [0, 100]$, $Y \in [-100, 0]$. We will also be interested in the way in which the structure of the solution depends upon β, which determines the nature of the relation between the overturning circulation and the density (salinity) contrast. According to the analysis by Hughes and Weaver (1994) using a three-dimensional ocean general circulation model, β is expected to be near 1. In our current work, we will loosely restrict the parameter range for β, and β will be varied through the sequence of values 1.0, 1.2, 1.4, and 1.6. As shown later, the structure of the solution changes drastically as β increases. Another parameter that will prove to have interesting effects is μ, which modifies the contribution of diffusion to some extent. This parameter will be varied through the sequence 0.3, 0.5, and 0.7 for the purpose of sensitivity analysis.

The equilibrium solutions of our dynamical systems model of the North Atlantic THC may be classified into three categories. One category corresponds to the condition $y \leq 0$. This category corresponds to solutions in which NADW formation effectively ceases and it will hereafter be referred to as the *stagnant regime*. The second and third categories have equilibrium solutions in $y > 0$. Figure 2 shows the equilibrium solutions for

Downloaded from http://journals.ametsoc.org/jcli/article-pdf/12/8/2238/3775210/1520-0442(1999)012_2238_adsmot_2_0_co_2.pdf by guest on 15 June 2020

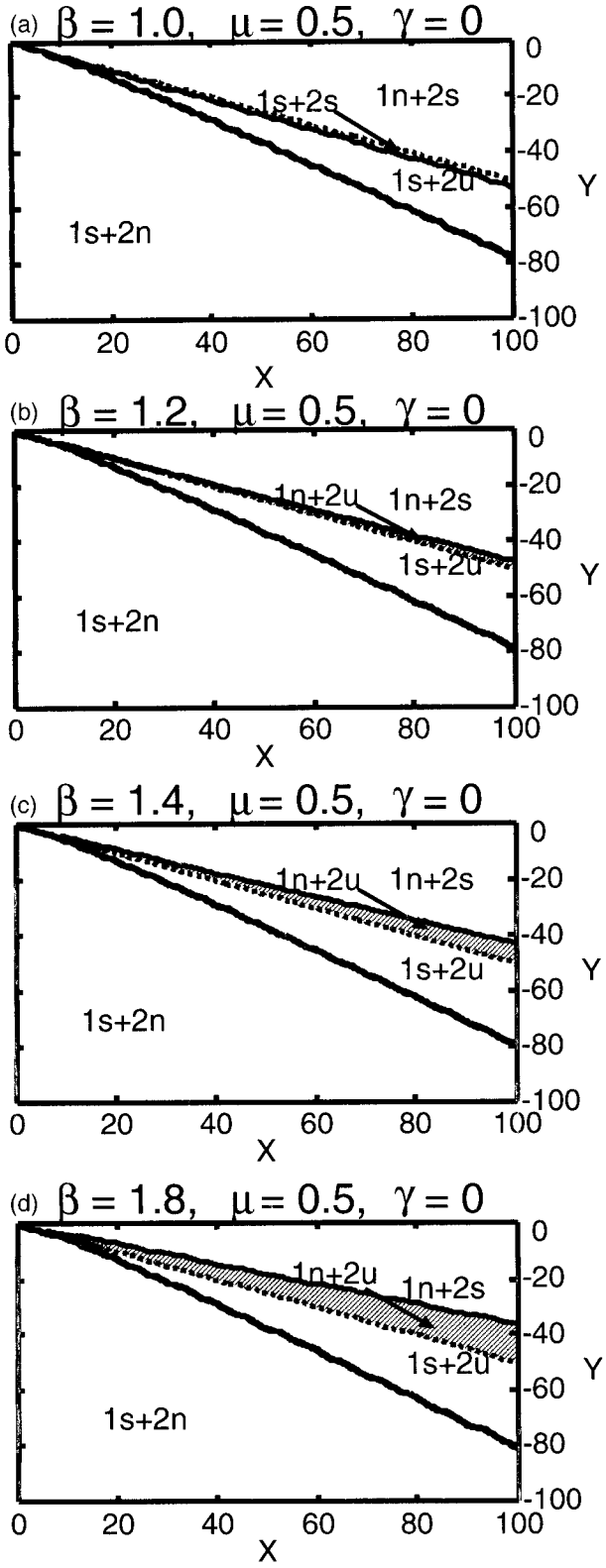

FIG. 3. Solution classification diagrams over the parameter space of X and Y. Two regimes are presented: one is the intense NADW forming regime, which has stable solutions when $-Y$ is relatively small, and the other is the stagnant NADW regime (linear regime), which has stable solutions when $-Y$ is set relatively large. From the top to bottom panels, β is varied through the sequence as (a) 1.0, (b) 1.2, (c) 1.4, and (d) 1.6, respectively; μ is held fixed to 0.5. The numbers and letters in each region indicate the corresponding status of the solutions within the domains separated by the lines of demarcation; the number 1 indicates that the following (alphabetical) status index corresponds to the stagnant NADW state, whereas 2 denotes that it is that of the intense NADW formation state. The letters n, u, and s indicate the status of the solution respectively as nonphysical, unstable, and stable. The dashed lines denote the stability criteria ($Y + \mu X = 0$) for the linear regime, and the regime in which no stable equilibrium solution exists is shown as a hatched region.

y as a function of X and Y for two values of β in the $y > 0$ domain. In this region of parameter space the system allows multiple equilibria for some values of the parameters. Since the stagnant solution also exists for $Y + \mu X < 0$, at maximum three equilibria may exist simultaneously. We classify the $y > 0$ solutions into two types: respectively, the *intense NADW formation* and the *weak NADW formation regimes*. The weak NADW formation regime, however, turns out to be always unstable over the range of control parameters investigated, and the discussion of solution regimes will focus upon these two (possibly stable) regimes, that is, the stagnant regime and the intense NADW formation regime, unless explicit mention is made to the contrary.

Figure 3 summarizes the classification of solutions on the XY plane when $\mu = 0.5$ and for a value of the parameter $\gamma = 0$ (the definition and physical meaning of γ will be introduced shortly). On the figure, the results are shown for four different values of β. The situation for the case $\beta = 1$ is shown in the top plate. Clearly evident is the fact that the local stability of the equilibrium solution of the dynamical system is split into two regimes by the condition $Y + \mu X = 0$: when $Y + \mu X < 0$, only solutions in the stagnant regime are stable, and when $Y + \mu X > 0$, only solutions in the intense NADW formation regime are stable (the line $Y + \mu X = 0$ is plotted as dashed). The nomenclature employed in this figure is such that the number 1 refers to the stagnant steady state, whereas the number 2 refers to the state of strong NADW formation. Each of these states is classified as either s (steady), u (unsteady), or n (nonphysical) in each of the regions into which the X–Y plane is divided.

Near the value $\beta = 1.2$, a Hopf bifurcation occurs for a value of Y slightly smaller than $-\mu X$. In Fig. 3b the intense NADW formation regime becomes unstable for a value of Y just below $-\mu X$. As we have discussed previously, in the absence of a stable equilibrium solution, even if it is only locally stable, the solution obtained by direct integration should become either a simple orbit or a chaotic orbit in phase space. The existence of the region of parameter space in which no stable equilibrium solutions exist is more clearly visible in parts Figs. 3c,d.

Downloaded from http://journals.ametsoc.org/jcli/article-pdf/12/8/2238/3775210/1520-0442(1999)012_2238_adsmot_2_0_co_2.pdf by guest on 15 June 2020

The forcing applied to the low–midlatitude NA, X, may not have experienced any significant change even under glacial conditions, as assumed in SP96 and SP97, and thus it may suffice to consider only one particular value of X in Fig. 3; as is evident from the figure, the stability structure does not significantly change when Y/X is constant. According to the hypothesis in SP96 concerning the hydrological cycle, the high-latitude NA was subject to anomalously high freshwater flux under full glacial conditions due to the existence of the huge Laurentide ice sheet that covered all of Canada (the Fennoscandian ice sheet is also expected to have contributed to high-latitude freshening); therefore we might imagine Y to change somewhat proportionally to ice sheet coverage. When $-Y$ remains small, at least a locally stable equilibrium solution exists and the system may settle onto the *equilibrium point.* This situation coincides with the modern NA THC in the dynamical systems model and reproduces exactly the same situation as that described in SP96. When $-Y$ become large, but not so large that the system allows only the stagnant solution, the reduced dynamical systems model of the NA THC has no stable equilibrium solution but may perhaps deliver a limit cycle as we shall see. This bifurcation structure is very similar indeed to that revealed in the considerably more complicated model of SP96, and we may therefore claim that the dynamical systems model developed herein accurately captures the essential mechanism of the millennial timescale oscillation previously revealed. Typical integrations of the model to be discussed in the next section will demonstrate that, beyond the bifurcation point, the model delivers the same millennium timescale oscillation as that obtained in the more complicated model of SP96.

A further set of sensitivity experiments has also been performed and is summarized in Fig. 4. In this set, μ is varied between 0.3 and 0.7, whereas β is held fixed to 1.4. One can clearly see that increasing μ causes enlargement of the range of forcing parameters for which the condition of unstable solution exists for the intense NADW formation regime. When $\mu = 0.3$, not only does the reduced dynamical system always have stable equilibrium solutions but it also allows stable multiple equilibria. When $\mu = 0.7$, on the other hand, the domain of unstable solutions for the intense NADW formation regime becomes noticeably larger.

In a first set of sensitivity tests we have set $\beta = 1.4$ (see Fig. 4) in order to view a region of parameter space in which no stable equilibrium solutions exist as *standard.* We would nevertheless have the unstable domain even when $\beta = 1$ for a large region in X–Y parameter space if μ were set to be sufficiently larger than 0.5. Since μ is the ratio of the local rate of diffusive exchange (between x, y, and z) to the global rate [here global implies between one of (x, y, z) and the background] of diffusive exchange, increasing μ means that the diffusive exchange among x, y, and z is more important than diffusive exchange between the main res-

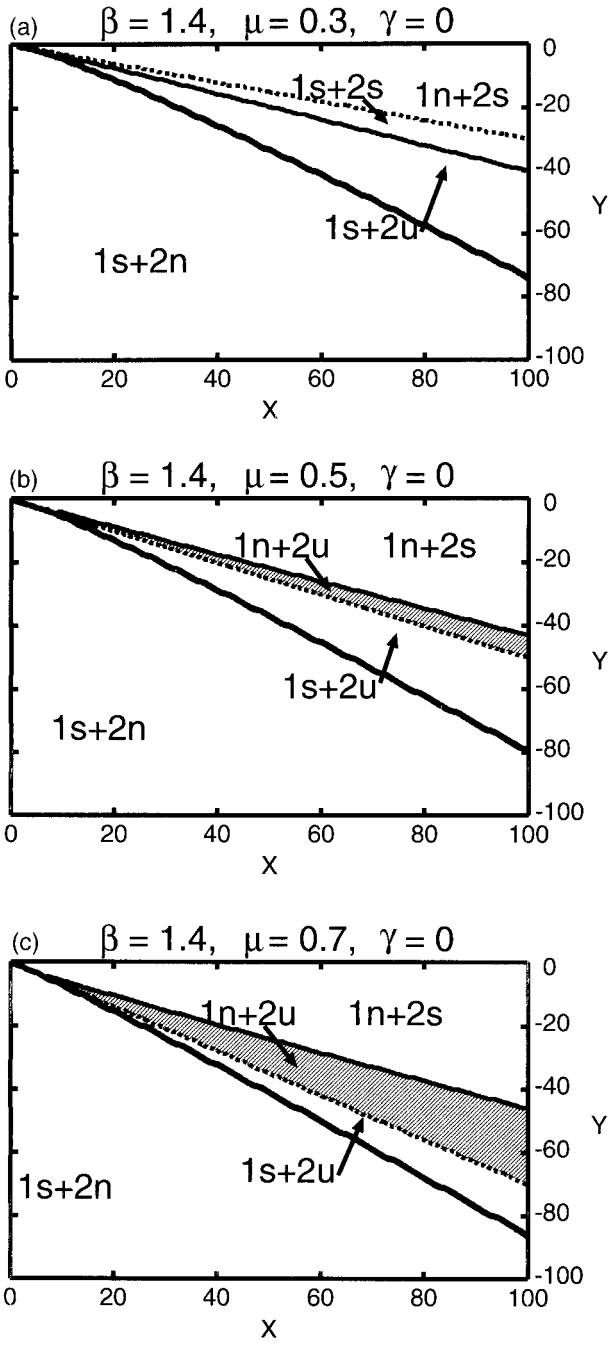

FIG. 4. Solution classification diagrams over the parameter space of X and Y. Two regimes are presented: one is the intense NADW forming regime, which has stable solutions when $-Y$ is relatively small, and the other is the stagnant NADW regime (linear regime), which has stable solutions when $-Y$ is relatively large. From the top to bottom panels, μ is varied through the sequence as (a) 0.3, (b) 0.5, and, (c) 0.7, respectively; β is held fixed to 1.4. The meaning of the numbers and letters in each panel is the same as in Fig. 3. The dashed lines denote the stability criteria ($Y + \mu X = 0$) for the linear regime, and the regime in which no stable equilibrium solution exists is shown as a hatched region.

Downloaded from http://journals.ametsoc.org/jcli/article-pdf/12/8/2238/3775210/1520-0442(1999)012_2238_adsmot_2_0_co_2.pdf by guest on 15 June 2020

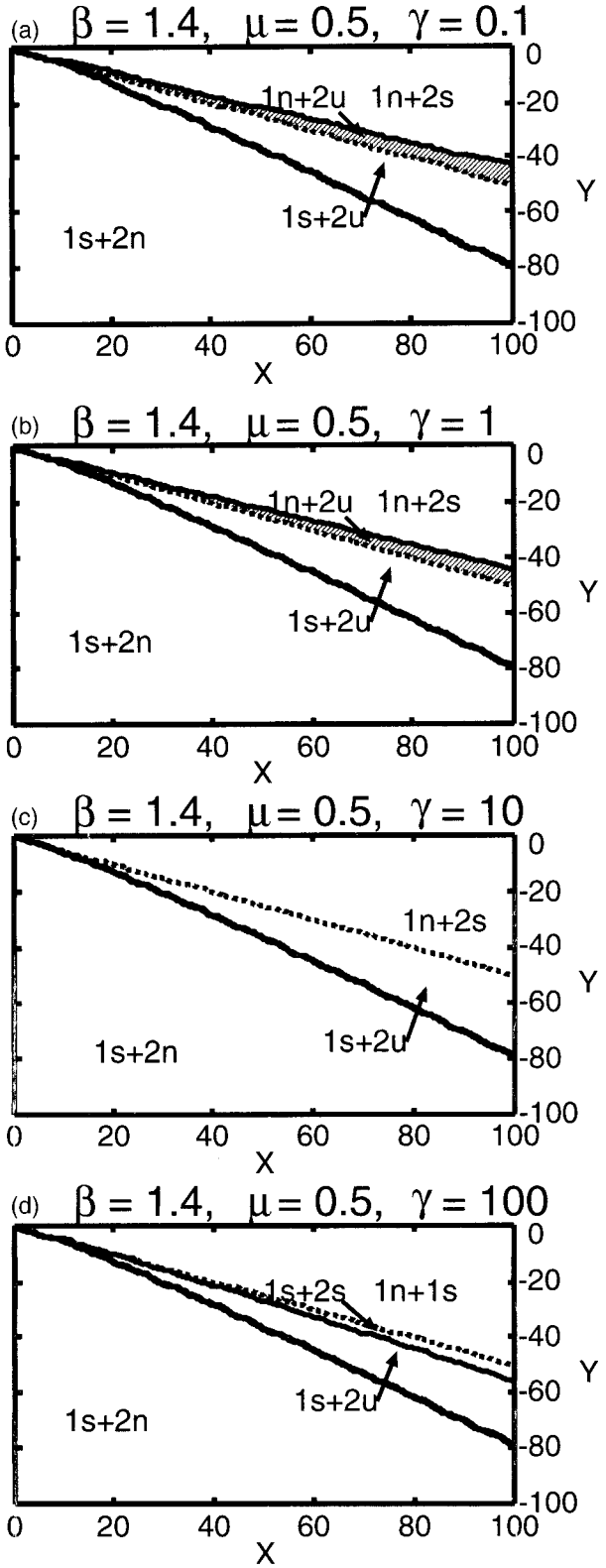

FIG. 5. Solution classification diagrams over the parameter space of X and Y. Two regimes are presented: one is the intense NADW forming regime, which has stable solutions when $-Y$ is relatively small, and the other is the stagnant NADW regime (linear regime), which has stable solutions when $-Y$ is relatively large. From the top to bottom panels, γ is varied through the sequence (a) 0, (b) 1, (c) 10, and (d) 100, respectively; β is held fixed to 1.4 and μ to 0.5. The meaning of the numbers and letters in each panel is the same as in Fig. 3. The dashed lines denote the stability criteria ($Y + \mu X = 0$) for the linear regime, and the regime in which no stable equilibrium solution exists is shown as a hatched region.

ervoir and the background. Although determination of the most realistic value of μ must await further investigation, this case study suggests to us that over a rather wide range of parameters the space contains a domain in which no stable equilibrium solutions exist and in which a limit cycle should characterize the nature of the solution.

It is well worth pointing out that the Hopf bifurcation is also suppressed and the system thereby stabilized when we add an additional term to Eq. (9) of the form $-\gamma(z - x)$, where $\gamma \geq 0$. This term obviously tends to reduce the difference between y and z. For sufficiently large γ, the system is then expected to behave very similarly to Stommel's box model (Stommel 1961) in which no such limit cycle exists.

Figure 5 summarizes the results of the analysis that are obtained when we apply nonzero γ to the reduced dynamical systems model of the NA THC. As one will clearly observe in Fig. 5, the region of parameter space in which only unstable solutions for the intense NADW formation regime exists shrinks, as γ is increased from 0 to 100. In the bottom panel of Fig. 5, another parameter domain in which stable multiple equilibria exist will be observed.

These analyses demonstrate that the spatial heterogeneity of NADW that drives the NA THC plays the central role in the instability. Since it is rather unnatural to imagine that the NADW domain is perfectly well mixed so as to have homogeneous density, and its heterogeneity has indeed been demonstrated in two-dimensional models such as that of SP96 and in three-dimensional models such as that of Winton and Sarachik (1993), we have included this heterogeneity explicitly and shown it to be critical to the physical phenomenon of interest. This analysis also clarifies the existence of orbital solutions of the dynamical systems model when the freshening of the high-latitude NA is close to the critical level above which it would suppress the NADW formation process entirely.

4. Sample integrations

An important result obtained on the basis of the linear analysis is that the system contains a transition from a locally stable point attractor to unsteady bounded solutions via a Hopf bifurcation. The bifurcation occurs when $\beta > 1.2$ and $Y + \mu X \gtrsim 0$ if $\mu = 0.5$. In order to examine the fully nonlinear behavior of the system, in this section we will illustrate the results obtained on

Downloaded from http://journals.ametsoc.org/jcli/article-pdf/12/8/2238/3775210/1520-0442(1999)012_2238_adsmot_2_0_co_2.pdf by guest on 15 June 2020

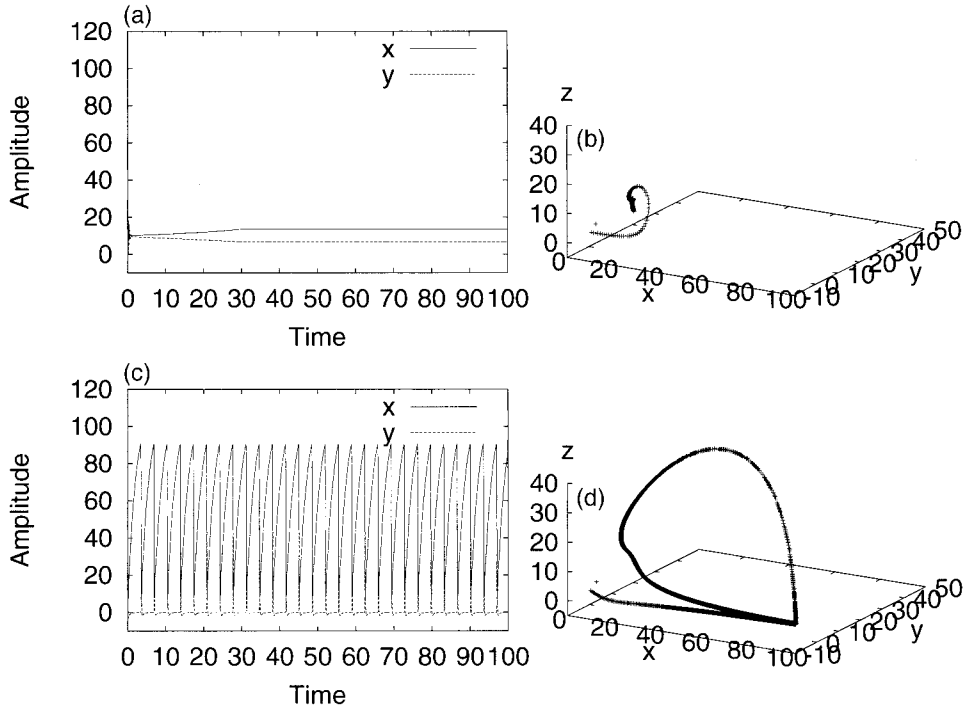

FIG. 6. Two integrations of the reduced dynamical system of the North Atlantic thermohaline circulation when the transport is linearly proportional to the salinity difference between NADW and the background. The equilibrium solution is locally stable. Two cases differ only by the initial conditions: Upper panels show [left: time series of x and y; right: phase space trajectory of (x, y, z)] the result when the initial value is close to the stable equilibrium solution, whereas the lower panels show the result when the initial condition is set far from the equilibrium solution. X, Y, μ, and γ are held fixed to 100, -45, 0.5, and 0, respectively.

the basis of direct numerical integrations of the governing system (7), (8), and (9). In the results that are presented in this section, all the model parameters except β are held fixed: namely, we will assume $\mu = 0.5$, $\gamma = 0$, $X = 100$, and $Y = -45$.

a. Solutions corresponding to linear transport: The case $\beta = 1$

For the simplest case in which the power law exponent is set to unity, the equilibrium solutions for either the stagnant or intense NADW regimes are locally stable whatever the combination of X and Y in the investigated range. For the linear case (the stagnant regime, $Y + \mu X < 0$) it is true that the equilibrium solution is a global attractor. For the nonlinear regime ($Y + \mu X > 0$), it is not guaranteed that the equilibrium solution will be a global attractor.

Figure 6 presents sample integrations for the case when $\beta = 1$. Figures 6a,b present the result obtained when the system is initialized near the equilibrium point. Expectedly, the solution converges onto the local equilibrium solution corresponding to the regime of intense NADW formation. On the other hand, Figs. 6c,d exhibit an obvious oscillation. The oscillation is on a timescale that is several times larger than the characteristic timescale for diffusion, and the shape of the oscillation is very similar to that delivered by the model of SP96 and connected to the Dansgaard–Oeschger oscillation. The only difference between the result shown in the lower part of Fig. 6 and that in the upper part involves the initial conditions. In the second example, the dynamical systems model of the NA THC was initialized far from the equilibrium solution and in this circumstance direct integration shows that it remains removed from the equilibrium solution.

These results for the case of *linear transport* demonstrate that our dynamical systems model of the NA THC may deliver *millennial timescale* oscillations even when the equilibrium solution corresponding to the intense NADW formation regime is linearly stable. It is also important to note how easy it is with the model to produce a millennium timescale oscillation that is very similar to the Dansgaard–Oeschger mode that is predicted by the model of SP96 under similar circumstances. The linear analysis of the equilibrium solutions presented in the previous section shows that even when $\beta = 1$, in which case the dynamical systems model best approximates that of SP96, the model possesses a region of parameter space in which no stable equilibrium solutions exist when $\mu > 0.5$ (not shown). Here we have shown that even under conditions such that the equilibrium solution in the intense NADW formation regime

Downloaded from http://journals.ametsoc.org/jcli/article-pdf/12/8/2238/3775210/1520-0442(1999)012_2238_adsmot_2_0_co_2.pdf by guest on 15 June 2020

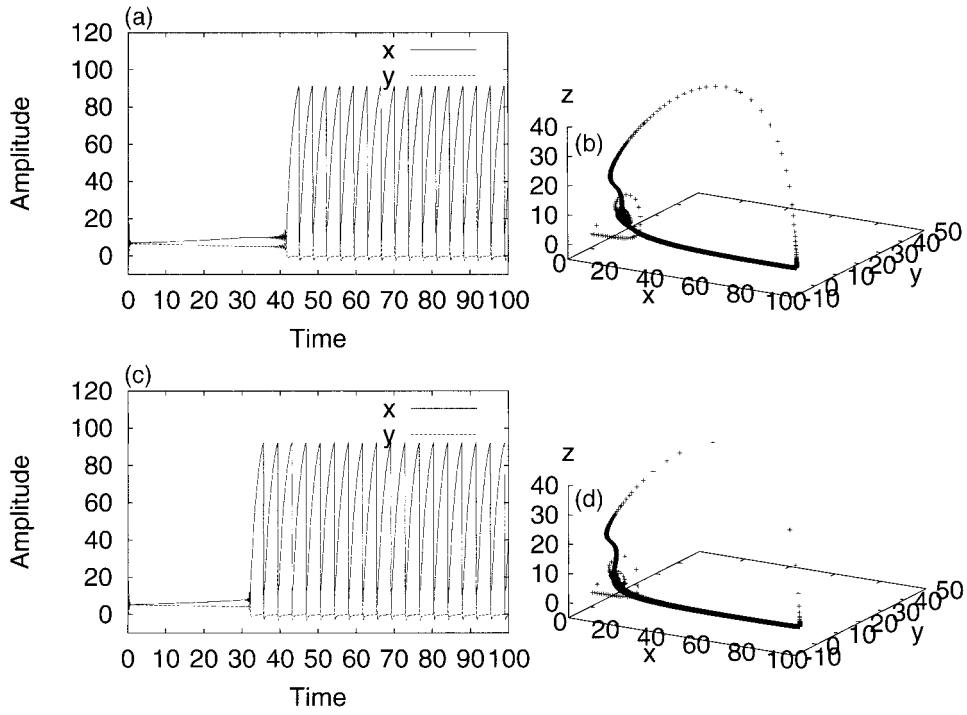

FIG. 7. Integrations of the dynamical system when the overturning transport is superlinearly proportional to salinity difference. The equilibrium solutions are locally unstable. The upper panel shows the case when $\beta = 1.4$, whereas the lower panel shows that of $\beta = 1.8$. For each case, the system is initialized near the stable equilibrium solutions. X, Y, μ, and γ are held fixed to 100, -45, 0.5, and 0, respectively.

is locally stable, the system may nevertheless not converge to the equilibrium solution, but rather may remain on a limit cycle orbit in phase space.

b. *Solutions with nonlinear transport: The cases $\beta > 1$*

When β is larger than unity, we may expect some modification of the solutions obtained with linear transport. Figure 7 presents the results obtained on the basis of two representative integrations of the dynamical systems model in this regime. In these two experiments, the initial values of (x, y, z) were initialized near those corresponding to the equilibrium solution, but the phase space trajectory is still repelled from the equilibrium since this is no longer locally stable, and the trajectory eventually forms a limit cycle that is illustrated on the phase space diagram. It will be observed that the evolution of the trajectory in each cycle of the oscillation is essentially the same as in the oscillation that occurs in the linear case ($\beta = 1$), and of course it is very similar to the results obtained using the considerably more complicated model in SP96.

The oscillation is apparently characterized as possessing two distinct stages in each cycle of the millennial timescale oscillation: a stagnant stage, which occupies most of the period of the cycle, and a very intense NADW forming stage. Since the period during which x decreases rapidly in association with the intense transport accompanying the NADW formation process is rather brief, the period of the complete cycle is determined primarily by the duration of the stagnant stage. During the stagnant stage, x increases gradually, in a way that is determined by the balance between X and Y as expressed in (7) and (8), toward a virtual *equilibrium* state that lies in the $y \geq 0$ domain.

c. *Spectral analyses of the integrations for $\beta = 1.4$*

It is of interest to consider the impact upon the period of the millennial timescale oscillations delivered by the dynamical systems model of the THC due to changes of the high-latitude freshening parameter Y. One of the main results reported in SP96 and SP97 was that this period increased abruptly with the increase in freshening rate. In order to answer this question, we have performed a spectral analysis of the y time series derived from integrations of the system when $\beta = 1.4$ for various values of Y for fixed $X = 100$.

Figure 8 summarizes the results obtained in this sequence of analyses. The oscillatory solutions exist in the range of $-Y$ from near 40 to 50. At $-Y \sim 40$, the period is approximately 2 in nondimensional time units. In dimensional time, with the diffusion timescale of 500 yr, 2 is equivalent to 1 kyr. As $-Y$ increases, the period increases to a value near 10 in nondimensional terms

Downloaded from http://journals.ametsoc.org/jcli/article-pdf/12/8/2238/3775210/1520-0442(1999)012_2238_adsmot_2_0_co_2.pdf by guest on 15 June 2020

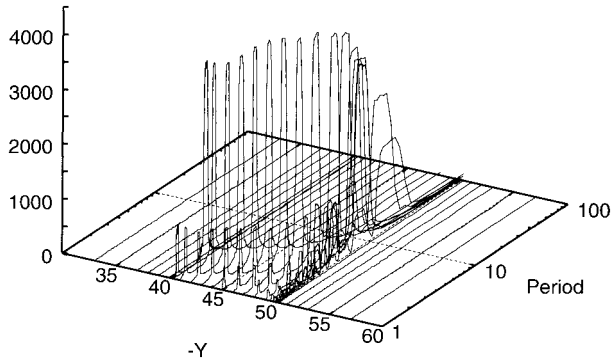

FIG. 8. Power spectra of the time series of y. X is held fixed to 100, β is held fixed to 1.4, μ to 0.5, and γ to zero. The horizontal axes are the period of power spectrum and the high-latitude forcing Y. Very high frequency perturbation (period ~1 yr) has been added, and the perturbation lowers the lower boundary of the Y parameter range in which the millennial timescale oscillations occurs.

near $-Y = 50$. In dimensional time this corresponds to a period of 5 kyr. Although our dynamical systems model is highly simplified, much more so even than the two-dimensional THC models employed in SP96 and SP97, the range of millennial timescale oscillations that is predicted by this model well fits the observed characteristics of the Dansgaard–Oeschger oscillation as well as the results obtained with our previously discussed models.

5. Response to periodic perturbations

To this point we have established that the dynamical systems model does capture the essence of the D–O oscillation. If the system were structurally unstable, however, we would be in no position to conclude that the mechanism embodied in the model was correct, apparently because we have ignored many other climate processes on various timescales in the process of formulation of the multibox model. Furthermore, to this point we have yet to consider the impact on the oscillations of external perturbations such as that associated with the annual cycle as well as, on very long timescales, possible oscillations of the continental ice sheet–climate system. In order to demonstrate the considerable robustness of the D–O regime in our model we will herein consider the behavior of the system when it is subject to perturbation, in particular to periodic forcing of prescribed amplitude.

Two different types of periodic forcing will be considered: one that is sinusoidal and a second that is asymmetric and of sawtooth form. In each experiment, the amplitude of the perturbation is held fixed to values comparable to X, a fairly large value considering the amplitude of annual evaporation minus precipitation (and runoff from the continents).

a. The response to sinusoidal perturbation

In a first set of experiments to investigate the impact on the response of time-dependent forcing, we have added an excitation of the form $A \sin\omega t$ to the dynamical system so as to scan a range of amplitudes and frequencies. The perturbation is applied solely to the high-latitude domain, the representative variable for which is y, considering that it is likely that the largest changes to freshwater forcing occurred at the surface of the high-latitude NA in association with the enhanced freshwater forcing that was most probably characteristic of glacial conditions (e.g., Crowley and North 1991).

The basic configuration of the system employed in the context of these perturbation experiments has been held fixed to a condition specified by the control parameters $\beta = 1.4$, $\mu = 0.5$, and $\gamma = 0$, and the forcing parameters to $X = 100$ and $Y = -45$. In this state the unperturbed model delivers a solution characterized by a typical millennial timescale oscillation. The amplitude of the perturbation added to this system was varied through the sequence $0.1X$ (=10), $0.5X$ (=50), and X (=100). Considering that these perturbations are of comparable strength to the *boundary forcing* X and Y, it is clear that the system must be considered to be strongly perturbed in these experiments. The frequency of the applied perturbation was also varied over the range from 0.01 to 100 measured in terms of the characteristic timescale of diffusion. This range corresponds to a dimensional range of timescale from 5 yr to 50 000 yr when the characteristic timescale of diffusion is 500 yr.

Figure 9 shows a summary of the results obtained in these experiments. On each of the three panels that show the results for the three different choices of forcing amplitude, the power spectra of the y time series are plotted for different forcing periods. It will be noted that even when the amplitude of the forcing is set to 10, the necessary condition for the occurrence of the millennium timescale oscillation is always violated near the extrema of the sinusoidal perturbation.

It is clearly shown in Fig. 9 that the behavior of the system is radically transformed for a value of the period of the forcing of unity in which case the period of the applied perturbation coincides with the characteristic timescale for diffusion. When the period of the applied

→

FIG. 9. Response of the dynamical system when sinusoidal perturbations are applied to the high-latitude NA with various periods. The amplitude of the perturbation is held fixed to a certain portion of X. The top panel shows the case when the amplitude is set to $0.1X$ (=10), the middle panel shows the case when the amplitude is set to $0.5X$ (=50), and the bottom panel shows that of the amplitude set to X (=100). Power spectra are shown in terms of the period of the perturbation and the period of the resulting time series. Power spectra, the

Downloaded from http://journals.ametsoc.org/jcli/article-pdf/12/8/2238/3775210/1520-0442(1999)012_2238_adsmot_2_0_co_2.pdf by guest on 15 June 2020

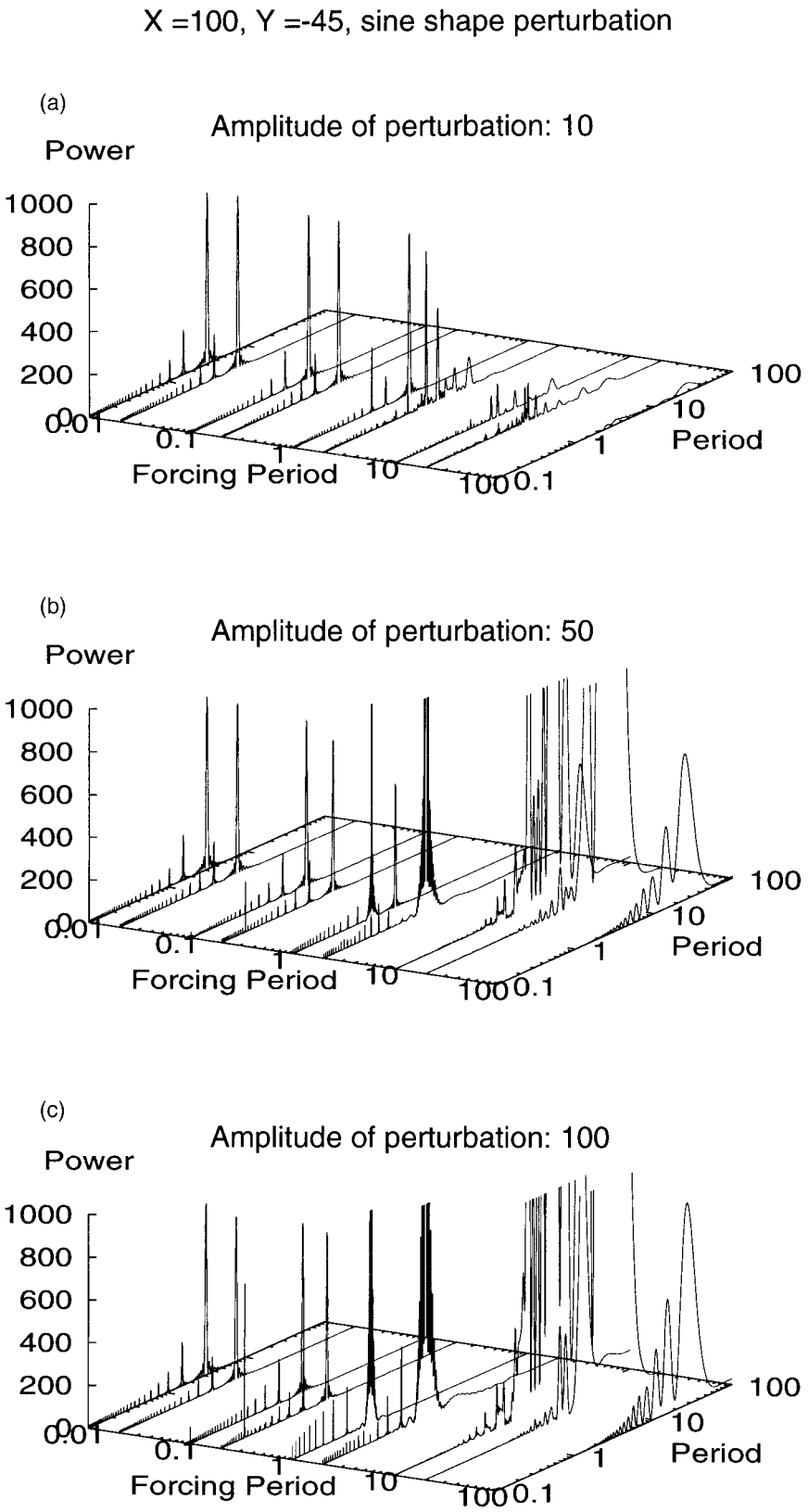

amplitude of which exceed 1000, are out of the scope and therefore not shown in the lower two panels.

Downloaded from http://journals.ametsoc.org/jcli/article-pdf/12/8/2238/3775210/1520-0442(1999)012_2238_adsmot_2_0_co_2.pdf by guest on 15 June 2020

harmonic perturbation is shorter than 1, the same millennial timescale oscillation exists even when very large amplitude perturbations are applied, whereas the box model of the NA THC becomes locked to the period of the forcing when this is longer than the characteristic timescale of diffusion.

These results strongly suggest that the mechanism of the millennial timescale oscillation of the NA THC is extremely robust against periodic excitation when the period of this excitation is shorter than the characteristic timescale of diffusion. The annual cycle, for example, satisfies this condition, and even the century timescale variability that may exist in systems with more degrees of freedom, such as that discussed, for example, in SP96, also satisfies this condition. As we have demonstrated through linear stability analysis, the millennial timescale oscillation may exist over a very wide range in control parameter space. The demonstrated robustness of the model produced D–O oscillation would appear, a posteriori, to further validate the model of the essence of this process developed herein.

b. The response to sawtooth perturbations: Implications for understanding the Bond cycle

In this section we will briefly describe a further series of results obtained with the dynamical systems model of the North Atlantic THC when it is perturbed with considerably longer timescale periodic perturbations. The motivation of this set of experiments was inspired both by the results obtained in SP96 and SP97, and by the analyses of Bond et al. (1993) of the information on late glacial climate contained in the Summit, Greenland, ice cores. According to the latter investigation, the region surrounding the high-latitude NA experienced a long timescale, sawtooth-shaped oscillation of temperature with a period of approximately 10 kyr, as well as the D–O oscillation itself. This longer timescale oscillation appears to be connected to the Heinrich events first described by Heinrich (1988), episodes during which large armadas of icebergs were apparently released from the Laurentide ice sheet on the east coast of North America, which were subsequently transported into the region of NADW formation by the North Atlantic drift. If some significant amount of Laurentide ice was removed in each such event, it would be expected to affect the NADW formation process in two different ways: first, anomalous freshwater flux associated with the ice rafting itself was undoubtedly applied to the high-latitude North Atlantic, which likely served to help suppress the process of NADW formation directly. Second, the removal of ice from the eastern flank of the Laurentide ice sheet may also have reduced the *non-sea level related contribution* to anomalous freshwater input onto the NA that is required to induce the D–O oscillation according to the hypothesis by SP96 and SP97. The first influence associated with the anomalous freshening accompanying the Heinrich events, however, acts on a timescale that is short compared to the period of the Bond cycle itself and may be best thought of as a several kyr period of very high freshwater flux. Since the bundling of the D–O oscillation within each of the Bond cycles can be observed throughout the decamillennium cycle, we, as a first attempt to investigate the origin of the Bond cycle with this highly simplified model, have ignored this influence. The second influence, on the other hand, might be expected to act over the entire duration of the Bond cycle, although this would also depend upon how much ice cover was removed by each of the Heinrich events. In this case, just prior to the initial sudden warming that initiates the Bond cycle, the North Atlantic would have been subject to maximum anomalous freshening. This qualitative description of the variation of anomalous freshwater forcing that is expected to have occurred through a typical Bond cycle suggests a simple sawtooth variation of this forcing. The dominant period of this variation would then have been on the 10-kyr timescale. With these considerations as motivation, we applied a sawtooth-shaped variation of freshwater flux to our dynamical systems model of the NA THC. Again, the control parameters were held fixed to $\beta = 1.4$, $\mu = 0.5$, and $\gamma = 0$. The forcing parameters were set to $X = 100$, and $Y = -41$ in this series of analyses. Figure 10 shows the z time series delivered by the dynamical systems model of the NA THC when this is subject to sawtooth periodic perturbations with various amplitudes. What is clearly observed in this sequence is the modulation of the millennial timescale Dansgaard–Oeschger oscillation on the longer timescale of the applied perturbation. When the amplitude of the perturbation is set to a large value, intense millennial timescale oscillations appeared only after each of the reductions in the strength of the freshwater perturbation, times that mimic the process that occurs at the end of a typical Heinrich event. Since the temperature proxy from Greenland ice cores indicates that somewhat weaker Dansgaard–Oeschger oscillations occur toward the end of each Bond cycle, the grouping of the millennial timescale oscillations predicted by the dynamical systems model does resemble, if crudely, the observed bundling of D–O oscillations that characterized the Bond cycle. This is, of course, based upon the assumption that episodes of intense NADW formation correspond to higher atmospheric temperature as discussed in SP97.

Before we will be entitled to conclude that the Bond cycle did in fact result directly from changes to the hydrological cycle associated with episodes of calving on the eastern flank of the Laurentide ice sheet associated with the Heinrich events, further analyses will clearly be required with more complete models of the process. Here we wish simply to put on record the suggestion that the Bond cycle may be thought as arising due to modulation by time-dependent meltwater forcing of a D–O oscillation that would exist under full glacial

Downloaded from http://journals.ametsoc.org/jcli/article-pdf/12/8/2238/3775210/1520-0442(1999)012_2238_adsmot_2_0_co_2.pdf by guest on 15 June 2020

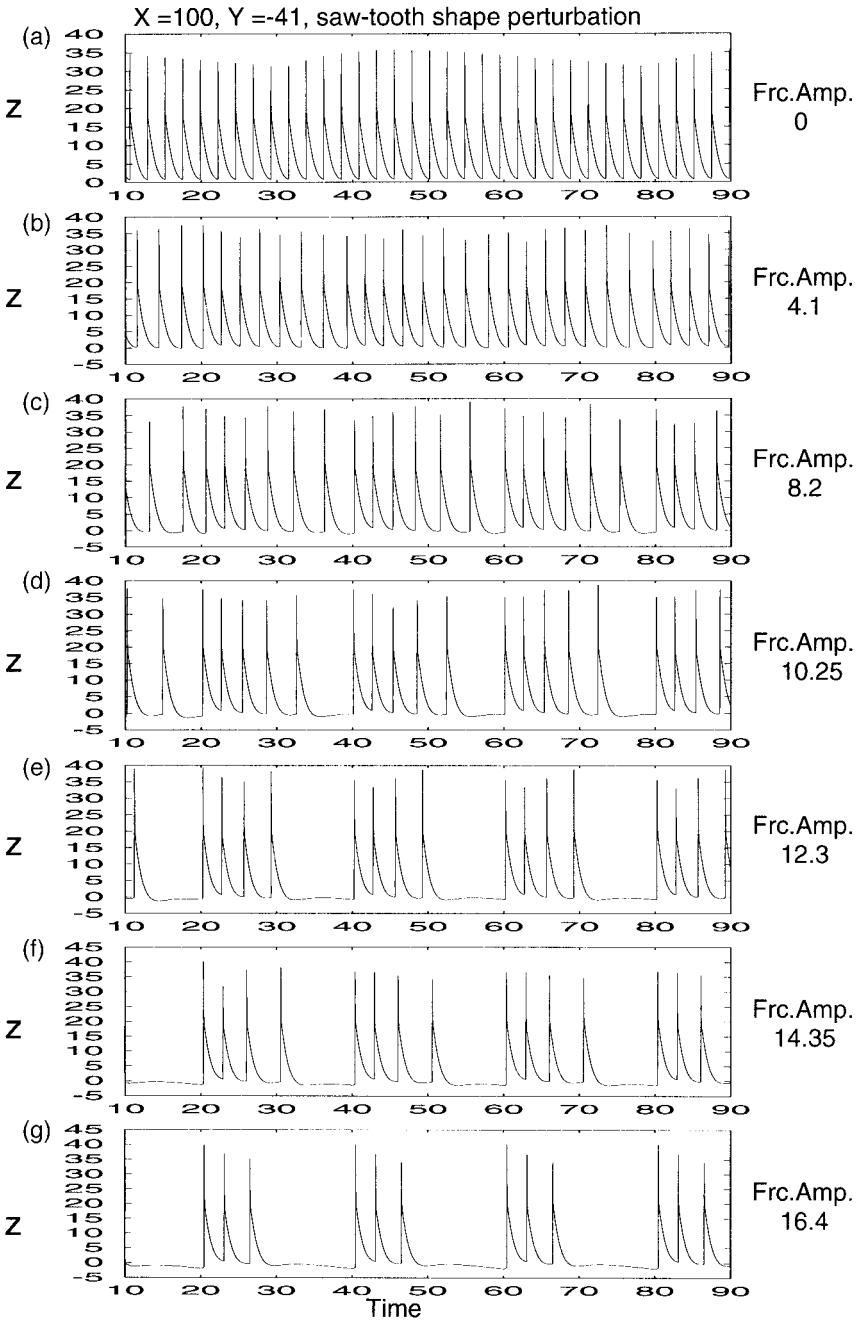

FIG. 10. Response of the reduced dynamical system of the NA THC when sawtooth-shaped perturbations are applied to the high-latitude NA with various amplitudes. The time series of z are plotted against time.

conditions even if the boundary conditions were time independent.

6. Conclusions

We have developed herein a low-dimensional dynamical systems model of the North Atlantic thermohaline circulation in order to provide further clarification of the mechanism that we have suggested to underlie the so-called Dansgaard–Oeschger oscillations that are so prominently observed during the late glacial stage of the last ice age cycle as this is recorded in Summit, Greenland, ice cores.

This reduced model apparently captures with some accuracy the evolving salinity distribution of the basin that has already been analyzed with the use of two- or

Downloaded from http://journals.ametsoc.org/jcli/article-pdf/12/8/2238/3775210/1520-0442(1999)012_2238_adsmot_2_0_co_2.pdf by guest on 15 June 2020

three-dimensional thermohaline circulation models such as those of Winton and Sarachik (1993) and Sakai and Peltier (1995, 1996). The simplified model is shown to reproduce important features of the mechanism of the Dansgaard–Oeschger oscillation that we have previously discovered in the course of work based upon two-dimensional thermohaline circulation models (SP96; SP97). In terms of the results obtained using coupled atmosphere–ocean systems, a further recent contribution by Winton (1997) has also provided an interesting insight on this issue, although the experiments performed in that work are based upon somewhat unrealistic assumptions. According to his analyses, the important factors that lead to the occurrence of the the D–O oscillation are the colder climate over the northern part of the North Atlantic basin and the very long relaxation time of sea surface temperature toward the reference temperature. There appears therefore to be a distinct difference between the recent suggestion of Winton (1997) and that embodied in the papers of Sakai and Peltier (1995, 1996, 1997). In our opinion the most essential ingredient that underlies the millennium timescale oscillation is common to both of these analyses, namely, the control exerted by freshwater forcing on the density of the surface water of the North Atlantic basin. By increasing the influence of the surface density flux relative to that of the boundary values, the THC system can be forced to oscillate, a bifurcation structure of THC systems that has been described in the earlier literature by, for example, Quon and Ghil (1992) and Sakai and Peltier (1993). Although most of the discussion in this paper has followed the previous work in SP96 and SP97 in focusing upon the important role applied by salinity forcing, an approach strongly motivated by the inference of Duplessy et al. (1991) to the effect that high-latitude NA salinity was strongly depressed during full glacial conditions, our theory of the millennium timescale THC oscillation would remain valid even if the role of the temperature field were to prove to be more important than we have assumed.

Our analysis of the dynamical systems model of the North Atlantic thermohaline circulation demonstrates that the Dansgaard–Oeschger oscillation has a simple structure that is driven by low–midlatitude salt accumulation and controlled by freshening in the northern portion of the basin where deep water is formed. The millennial timescale oscillation can exist even if the equilibrium solution is locally stable when the overturning transport in the reduced system is linearly dependent upon the density contrast, and the oscillation is inevitable when the overturning transport is superlinearly dependent upon the density contrast. The period of the oscillation ranges from a millennium to several millennia, and the oscillation appears only when the intensity of high-latitude freshening is slightly weaker than that required to shut down the overturning circulation entirely. This is fully consistent with the results reported in SP96 and SP97.

We have also reported a series of analyses concerning the way in which the variability of the deep circulation is modified when the buoyancy forcing is time dependent. These analyses have established that the model of the Dansgaard–Oeschger oscillation is extremely robust against relatively short timescale perturbations, but that the system is easily modulated by relatively long timescale perturbations. On the basis of the latter results we have suggested that the Bond cycle (Bond et al. 1993) is simply a consequence of the variation of the freshwater forcing applied to the North Atlantic in association with Heinrich events. A marked difference in the nature of the response to periodic forcing occurs when the forcing timescale exceeds the diffusion timescale compared to that that obtains when the forcing timescale is less than the diffusion timescale.

A very recent analysis of paleoceanographic data by Bond et al. (1997) has provided very interesting and potentially important new information on millennium timescale climate variability. According to these analyses the North Atlantic has experienced millennium timescale variability even during the current Holocene epoch following deglaciation. Although this variability is much weaker than the glacial D–O oscillation, it appears to be characterized by the same timescale. GRIP (1993) and GISP2 (1993) analyses and our previous analyses using an ice age climate model have shown that the glacial millennium timescale oscillation is accompanied by a large-amplitude temperature oscillation that is not observed during the Holocene. We therefore suggest that the mechanism underlying the Holocene millennium timescale variability may well be different from that responsible for the millennium timescale oscillation that occurred under full glacial conditions.

Acknowledgments. The research reported in this paper is a contribution to the Canadian national programme in Climate System History and Dynamics, which is funded by the Natural Sciences and Engineering Research Council of Canada and by the Atmospheric Environment Service of Canada. Additional research support was provided from NSERC Grant A9627 to WRP.

REFERENCES

Birchfield, G. E., and W. S. Broecker, 1990: A salt oscillator in the glacial Atlantic? 2. A ''scale analysis'' model. *Paleoceanography,* **5,** 835–843.

Bond, G., W. Broecker, S. Johnsen, J. McManus, L. Labeyrie, J. Jouzel, and G. Bonani, 1993: Correlations between climate records from North Atlantic sediments and Greenland ice. *Nature,* **365,** 143–147.

——, and Coauthors, 1997: A pervasive millennial-scale cycle in North Atlantic Holocene and glacial climates. *Science,* **278,** 1257–1266.

Broecker, W. S., G. Bond, and M. Klas, 1990: A salt oscillator in the glacial Atlantic? 1. The concept. *Paleoceanography,* **5,** 469–477.

Bryan, K., and L. J. Lewis, 1979: A water mass model of the world ocean. *J. Geophys. Res.,* **84,** 2503–2517.

Downloaded from http://journals.ametsoc.org/jcli/article-pdf/12/8/2238/3775210/1520-0442(1999)012_2238_adsmot_2_0_co_2.pdf by guest on 15 June 2020

Bunker, A. F., and L. V. Washington, 1976: Energy exchange charts of the North Atlantic Ocean. *Bull. Amer. Meteor. Soc.,* **57,** 670–678.

Crowley, J. T., and G. E. North, 1991: *Paleoclimatology. Oxford Monogr. on Geology and Geophysics,* No. 9, Oxford University Press, 339 pp.

Duplessy, J.-C., L. Labeyrie, A. Juillet-Leclerc, F. Maitre, J. Dupart, and M. Sarnthein, 1991: Surface salinity reconstruction of the North Atlantic Ocean during the last glacial maximum. *Oceanol. Acta,* **14,** 311–323.

Gargett, A. E., and B. Ferron, 1996: The effect of differential vertical diffusion of T and S in a box model of thermohaline circulation. *J. Mar. Res.,* **54,** 827–866.

GISP2, 1993: The 'flicking switch' of late Pleistocene climate change. *Nature,* **361,** 432–436.

GRIP, 1993: Climate instability during the last interglacial period recorded in the GRIP ice core. *Nature,* **364,** 203–207.

Heinrich, H., 1988: Origin and consequences of cyclic ice rafting in the Northeast Atlantic Ocean during the past 130,000 years. *Quat. Res.,* **29,** 142–152.

Hsiung, J., 1986: Mean surface energy heat fluxes over the global ocean. *J. Geophys. Res.,* **91,** 10 585–10 606.

Huang, R. X., and W. K. Dewar, 1996: Haline circulation: Bifurcation and chaos. *J. Phys. Oceanogr.,* **26,** 2093–2106.

Hughes, T. M. C, and A. J. Weaver, 1994: Multiple equilibria of an asymmetric two-basin ocean model. *J. Phys. Oceanogr,* **24,** 619–637.

Imbrie, J., and Coauthors, 1984: The orbital theory of Pleistocene climate: Support from a revised chronology of the Marine δ^{18}O record. *Milankovitch and Climate, Part 1,* A. L. Berger et al., Eds., D. Reidel, 269–305.

Johnsen, S. J., and Coauthors, 1992: Irregular glacial interstadials recorded in a new Greenland ice core. *Nature,* **359,** 311–313.

Keigwin, L. D., and G. A. Jones, 1994: Western North Atlantic evidence for millennial-scale changes in ocean circulation and climate. *J. Geophys. Res.,* **99,** 12 397–12 310.

Levitus, S., 1982: *Climatological Atlas of the World Ocean.* NOAA Professional Paper 13, 137 pp.

Marotzke, J., 1989: Instabilities and multiple steady states of the thermohaline circulation. *Oceanic Circulation Models: Combining Data and Dynamics,* D. L. T. Anderson and J. Willebrand, Eds., NATO ASI Series, Vol. 284, Kluwer Academic Publishers, 501–511.

Nakamura, M., P. H. Stone, and J. Marotzke, 1994: Destabilization of the thermohaline circulation by atmospheric eddy transports. *J. Climate,* **7,** 1870–1882.

Peixoto, P. J., and A. H. Oort, 1992: *Physics of Climate.* American Institute of Physics, 520 pp.

Quon, C., and M. Ghil, 1992: Multiple equilibiria in thermosolutal convection due to salt-flux boundary conditions. *J. Fluid. Mech.,* **245,** 449–483.

Sakai, K., and W. R. Peltier, 1993: Oscillatory modes of behavior in a simple model of the Atlantic thermohaline circulation. *Ice in the Climate System,* W. R. Peltier, Ed., NATO ASI Series, Vol. I-12, Springer-Verlag, 459–480.

——, and ——, 1995: A simple model of the Atlantic thermohaline circulation: Internal and forced variability with paleoclimatological implications. *J. Geophys. Res.,* **100,** 13 455–13 479.

——, and ——, 1996: A multi-basin reduced model of the global thermohaline circulation: Paleoceanographic analyses of the origins of ice-age climate variability. *J. Geophys. Res.,* **101,** 22 535–22 562.

——, and ——, 1997: Dansgaard–Oeschger oscillations in a coupled atmosphere–ocean climate model. *J. Climate,* **10,** 949–970.

Stommel, H. M., 1961: Thermohaline convection with two stable regimes of flow. *Tellus,* **13,** 224–230.

Stuiver, M., 1980: Solar variability and climatic change during the current millennium. *Nature,* **286,** 868–871.

Weaver, A. J., J. Marotke, P. F. Cummins, and E. S. Sarachik, 1993: Stability and variability of the thermohaline circulation. *J. Phys. Oceanogr.,* **23,** 39–60.

Winton, M., 1997: The effect of cold climate upon North Atlantic deep water formation in a simple ocean–atmosphere model. *J. Climate,* **10,** 37–51.

——, and E. S. Sarachik, 1993: Thermohaline oscillations induced by strong steady salinity forcing of an ocean general circulation model. *J. Phys. Oceanogr.,* **23,** 1389–1410.

Downloaded from http://journals.ametsoc.org/jcli/article-pdf/12/8/2238/3775210/1520-0442(1999)012_2238_adsmot_2_0_co_2.pdf by guest on 15 June 2020